Inhomogeneity of ^{13}C isotope distribution in isotope engineered carbon nanotubes: Experiment and theory

V. Zólyomi,[1,2] F. Simon,[3,4] Á. Rusznyák,[2] R. Pfeiffer,[3] H. Peterlik,[3] H. Kuzmany,[3] and J. Kürti[2]
[1]*Research Institute for Solid State Physics and Optics, Hungarian Academy of Sciences, P.O. Box 49, H-1525 Budapest, Hungary*
[2]*Department of Biological Physics, Eötvös University, Pázmány Péter sétány 1/A, H-1117 Budapest, Hungary*
[3]*Institut für Materialphysik, Universität Wien, Strudlhofgasse 4, A-1090 Wien, Austria*
[4]*Budapest University of Technology and Economics, Institute of Physics and Solids in Magnetic Fields Research Group, Hungarian Academy of Sciences, P.O. Box 91, H-1521 Budapest, Hungary*
(Received 24 October 2006; revised manuscript received 19 January 2007; published 15 May 2007)

Vibrational modes of ^{13}C isotope enriched single-walled carbon nanotubes are inhomogeneously broadened due to the random distribution of isotopes. We study this effect on the radial breathing mode theoretically using density-functional theory within the local-density approximation and compare the result with experiments on inner tubes in double-walled carbon nanotubes grown from ^{13}C-enriched fullerenes. Increased inhomogeneity was achieved by growing inner tubes from a mixture of enriched and natural fullerenes, which is explained by the calculations. This shows the absence of carbon diffusion along the tube axis during inner tube growth, supporting the theory of inner tube growth by Stone-Wales transformations from interconnected fullerenes.

DOI: 10.1103/PhysRevB.75.195419 PACS number(s): 78.30.Na, 71.15.Mb, 78.67.Ch

I. INTRODUCTION

Isotope engineering (IE) provides an important degree of freedom to study a range of phenomena which are relevant for both fundamental studies and applications. IE in general allows us to study effects which depend on the mass of nuclei while leaving the electronic properties unaffected. Examples, where IE has been successfully employed to understand fundamental phenomena, include phonon-mediated superconductivity,[1] identification of vibrational modes,[2–4] controlling heat conductivity properties using mononuclear Si,[5] and more recently the exciton-phonon coupling effect in single-walled carbon nanotubes.[6] An additional benefit of IE is that it allows us to select the nuclear moments and thus to enable nuclear magnetic resonance (NMR) studies on the materials. Recently, we prepared isotope-engineered carbon nanotubes which allowed Raman vibrational analysis[7] and NMR studies of the tube electronic properties.[8] Carbon nanotubes (CNTs) are the fourth phase of carbon after graphite, diamond, and fullerenes and are compelling materials with tubular structure and unique electronic properties. Depending on the number of concentric shells, CNTs can be single, double, or multiwalled. Single-walled carbon nanotubes[9,10] (SWCNTs) have, in particular, attracted significant interest due to the number of fundamental and application oriented properties such as, e.g., excitonic effects,[11,12] superconductivity,[13] the Tomonaga-Luttinger liquid state,[14,15] and the Peierls transition.[16,17] Conventional IE of SWCNTs considers the preparation from ^{13}C enriched graphite, which yields a material where other inevitably present carbon phases such as graphitic particles and amorphous carbon are also enriched.[18,19] This hinders both the reliable vibrational analysis and the NMR experiments.

The IE of carbon nanotubes with nanotube specificity was achieved by growing inner tubes from ^{13}C enriched fullerenes (C_{60},C_{70},...) encapsulated inside SWCNT host outer tubes.[7] Such double-walled carbon nanotubes (DWCNTs) are in general interesting due to the special growth environment realized inside the host SWCNTs for the inner tubes, which allows for the synthesis of remarkably high-quality inner tubes as evidenced by the narrow Raman linewidths.[20] Among other things, it has been shown that the outer tube remains intact during the formation of the inner tube.[7] Apart from the success of this synthesis, a number of open questions remain which concern the growth mechanism of inner tubes and the random distribution of the ^{12}C and ^{13}C isotopes. Two mechanisms have been suggested for the inner tube growth: (i) growth from dimerized or polymerized encapsulated fullerenes[21–23] through Stone-Wales transformations[24] and (ii) growth of inner tubes from completely disintegrated fullerenes, e.g., from C_2 vapor.[25] Note that although the carbon isotope distribution on the inner tube is random in both cases, this distribution correlates with the original distribution on the fullerenes only for the first mechanism. The random carbon isotope distribution was experimentally found to induce an inhomogeneous broadening of the Raman modes, which was best observed for the radial breathing mode (RBM) due to the large spectral spread and the narrow linewidth of this mode.[7] Calculations were found to explain the experimental data well.[7] However, as we present below, further experiments performed on samples that were produced by using a mixture of enriched and nonenriched fullerenes as filling material yielded a somewhat different behavior than the previous measurements: a larger broadening was found than expected. This prompted us to explore this phenomenon with a more careful analysis, and thereby possibly decide which of the two possible growth mechanisms is actually realized during synthesis.

In the following, we present calculations on the isotope distribution related inhomogeneous broadening for the RBM of ^{13}C-enriched inner tubes using density-functional theory within the local-density approximation on SWCNT cell sizes which are sufficient for convergence of the data. We synthesized two kinds of ^{13}C enriched inner tubes: made from ^{13}C-enriched fullerenes (uniform enrichment) and from mixtures of natural and ^{13}C-enriched fullerenes (mixed enrich-

ment). We observed that the RBMs are a factor of 3 more broadened for the mixed enrichment than for the uniform enrichment at the same overall enrichment levels. The relative difference is well reproduced by the calculations if inhomogeneous clustering of ^{13}C rich and poor regions are assumed along the inner tubes. A scaling of the data by a factor of 1.5–2 yields quantitatively accurate agreement between theory and experiment. The results presented here prove the absence of carbon diffusion along the tube axis during inner tube growth and are a strong support of inner tube growth through Stone-Wales transformations from preformed fullerene dimers or oligomers.

II. THEORY

We have applied density-functional theory at the local-density approximation level utilizing the projector-augmented-wave method using the Vienna *ab initio* simulation package[26–28] (VASP) to calculate the inhomogeneous broadening of the RBM mode for three SWCNTs that fall in the central part of the diameter distribution of the inner tubes: the (10,0), (7,4), and (5,5) nanotubes. As a first step, the Hessians of the nanotubes were calculated with VASP. We used a large plane-wave cutoff energy of 400 eV during the calculations. Geometries were optimized as in a previous work.[29] Long-range force constants were taken into account to ensure high accuracy of the frequencies. The lengths of the supercells used to calculate the Hessian matrices were 12.7 Å (three unit cells and 120 atoms), 13.6 Å (one unit cell and 124 atoms), and 14.7 Å (six unit cells and 120 atoms) for (10,0), (7,4), and (5,5), respectively. Force constants were derived from these Hessians. For some calculations, even larger supercells were needed. The Hessians for those calculations were constructed from the force constants calculated as written above; even longer-range force constants were safe to neglect as they are very small.

In order to calculate the inhomogeneous broadening for a given enrichment level, the RBM frequency had to be calculated by randomly distributing the ^{12}C and ^{13}C nuclei within the supercell while keeping the total number of ^{13}C nuclei fixed (as determined by the enrichment level). Therefore, the dynamical matrices of the tubes were constructed and diagonalized using a large number of different random distributions of ^{12}C and ^{13}C nuclei for the mass matrices. Once the RBM mode is obtained after the diagonalization, calculating the inhomogeneous broadening is a matter of calculating the standard deviation of RBM frequencies for all random isotope distributions.

However, identification of the RBM must be performed with caution. The presence of a large number of ^{13}C nuclei within the supercell results in a loss of symmetry and a distortion of the RBM mode. The distortion is significant, but the characteristic shape of the RBM—synchronized radial movement of nuclei—is largely retained (i.e., the distortion is basically a small modulation of the displacement of the atoms, such that the atoms do not all move with the same magnitude or in the same radial direction, unlike in the RBM normal mode, but they do all move in phase in a more or less radial direction), which allowed us to identify the RBM mode by means of a scalar product analysis. Let us denote the normal mode Cartesian coordinates of the ideal RBM mode of the pure SWCNT and the nth vibrational mode of the enriched SWCNT as $\{Q_i^{\mathrm{RBM}}\}$ and $\{Q_i^n\}$, respectively ($i=1,\ldots,3N$, where N is the number of atoms in the supercell). The scalar product $\Sigma_i Q_i^{\mathrm{RBM}} Q_i^n$ should be significant only in the case of the RBM-like modes[30]; thus, the RBM of the enriched SWCNT can be identified by calculating this scalar product.

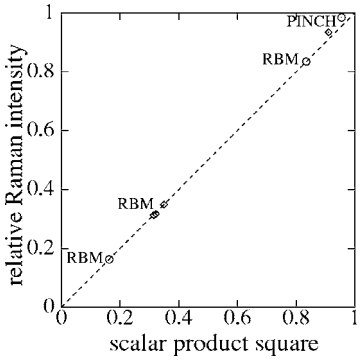

FIG. 1. Raman intensities (normalized to the mode intensities of $^{12}C_{60}$) of the pinch and radial breathing modes of C_{60} versus the w^n scalar product square of the distorted vibrational modes with the corresponding original modes for $^{13}C^{12}C_{59}$ (circles) and a randomly chosen $^{13}C_6{}^{12}C_{54}$ (diamonds). The points fit well to the $x=y$ line (dashed line), showing that w^n is a good approximation of the relative Raman intensities. Note that the RBM is already "split" for $^{13}C_1{}^{12}C_{59}$ due to the mixing of the RBM with other close energy vibrational modes. This effect is much smaller for the pinch mode, which is more separated from other modes in energy than the RBM.

The square of this scalar product can be used as a weight factor $w^n=|\Sigma_i Q_i^{\mathrm{RBM}} Q_i^n|^2$ in the intensity for the RBM of each isotope distribution.[30] We have performed a test calculation on C_{60} using the GAUSSIAN (Ref. 31) program package to see how well the square of the aforementioned scalar product can be matched to the relative Raman intensity of both totally symmetric modes of C_{60}. We calculated the vibrational modes and Raman intensities on the B3LYP/6–31G* level for C_{60} made purely of ^{12}C and for the case when one or six of the carbon atoms are (in the latter case randomly) replaced by ^{13}C. The results are depicted in Fig. 1, which show that the relative Raman intensities (normalized to the modes of C_{60} made of purely ^{12}C) are very well matched by the square of the scalar product of each vibrational mode with the corresponding nonenriched vibrational mode, both for the pinch mode and the radial breathing mode of C_{60}. Therefore, w^n could be used as a weight factor when calculating the standard deviation of the RBM frequency of SWCNTs.

III. EXPERIMENT

Commercial SWCNT material (Nanocarblab, Moscow, Russia[32]), ^{13}C isotope-enriched fullerenes (MER Corp., Tucson, USA), and fullerenes of natural carbon (Hoechst AG, Frankfurt, Germany) were used to prepare fullerene peapods C_{60}, C_{70}-SWCNT. The SWCNTs were purified by the supplier to 50 wt %. Such purity is sufficient to acquire good

quality Raman spectra in which the details are clearly visible, since Raman spectroscopy is highly selective for carbon nanotubes due to the resonance effect of the Van Hove singularities in the electronic density of states. The mean value of the tube diameter distribution as determined from Raman spectroscopy[33] is $d_{\text{mean}}=1.40$ nm, which is optimal for fullerene encapsulation. Two grades of ^{13}C-enriched fullerenes with nominal enrichment levels of $c=0.25$ and 0.89 were used; the actual enrichment levels in these samples were found to be $c=0.28$ and 0.82, respectively, as discussed below. (Note that in the present work, we use the latter, actual enrichment values in the labeling of the samples as it will be seen below, while in our previous work, we used the nominal enrichment in the labels,[7] but the corresponding fullerene samples are the same.) The 28% and the 82% grades were both composed of C_{60}/C_{70}/higher fullerene mixtures in relative proportions of 75%:20%:5% and 12%:88%:<1%. The natural carbon C_{60} ($^{\text{nat}}C_{60}$) had a purity of >99%. The ^{13}C content on the fullerenes follows a binomial distribution with probability p of finding n ^{13}C on a fullerene with $N=60,70$, or more carbons with $p(n\ ^{13}\text{C out of } N)=\binom{N}{n}c^n(1-c)^{N-n}$. For the fullerene encapsulation, the SWCNTs and the fullerenes were sealed under vacuum in a quartz ampoule and annealed at 650 °C for 2 h.[34] Fullerenes enter the SWCNTs at this temperature due to their high vapor pressure that is maintained in the sealed environment. We synthesized two different kinds of peapod materials: one where the encapsulated fullerenes were alike, i.e., from one enrichment grade and a mixture where the $c=0.28$ and the natural C_{60} were mixed in 1:1 concentrations prior to the filling. We denote the two kinds of peapod materials "uniform" and "mixed" fullerene-filled peapods, respectively. Nonencapsulated fullerenes were removed by dynamic vacuum annealing at the same temperature. The filling of SWCNTs was characterized by high-resolution transmission electron microscopy (HRTEM), by x-ray studies of the one-dimensional array of fullerenes inside the SWCNTs, and by the detection of the fullerene modes from the cages encapsulated inside the SWCNTs using Raman spectroscopy.[34]

The peapods were transformed to DWCNTs by a dynamic vacuum treatment at 1250 °C for 2 h following Ref. 35. The DWCNT transformation was followed by HRTEM and by the observation of the DWCNT structure factors with x-ray studies. In addition, new Raman modes emerge after the transformation particularly in a frequency range that is upshifted from the outer tube RBMs. According to the more or less $1/d$ scaling of the RBM modes,[29] where d is the tube diameter, these lines are an additional proof for the growth of the small diameter inner shell tubes.[20,35] DWCNTs based on the uniformly filled peapods with different ^{13}C enrichment grades are denoted as $^{\text{nat}}C$-, $^{13}C_{0.28}$-, and $^{13}C_{0.82}$-DWCNT. The DWCNT based on the fullerene mixture is denoted as $^{13}C_{0.15-M}$-DWCNT, which reflects its $c=0.15$ enrichment level, which is discussed below. Vibrational analysis was performed on a Dilor xy triple Raman spectrometer in the 1.64–2.54 eV (676–488 nm) energy range at 90 K. The spectral resolution was 0.5–2 cm^{-1} depending on the laser wavelength and the resolution mode used (high or normal resolution). For the DWCNT RBM linewidth analysis, we used the 676 nm laser line where the spectrometer resolution is as high as 0.5 cm^{-1} in the high-resolution mode.

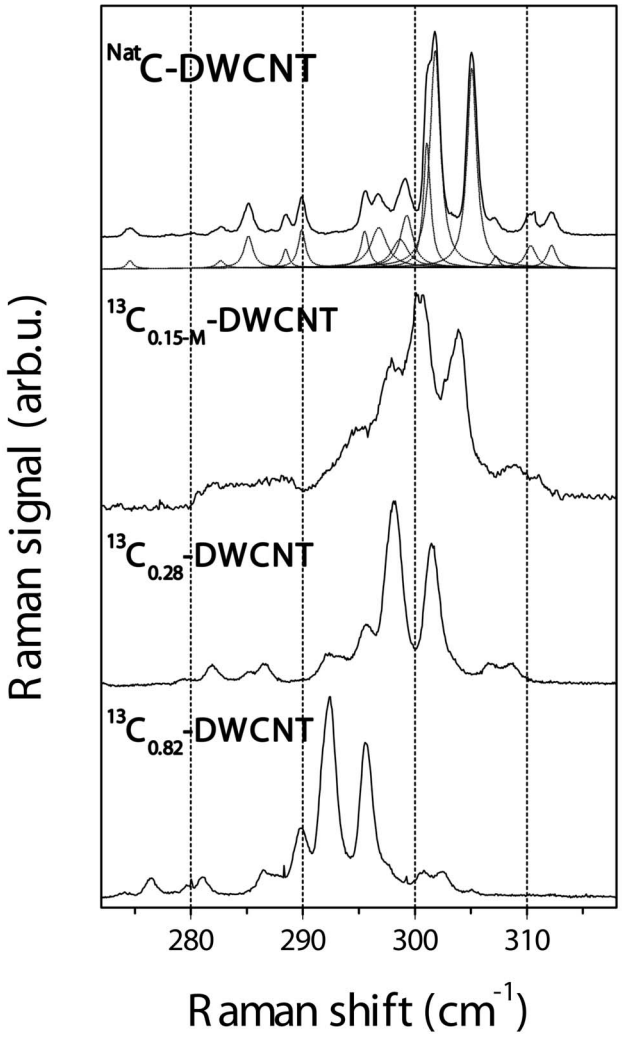

FIG. 2. Measured Raman spectra (solid lines) of DWCNTs with $^{\text{nat}}C$, $^{13}C_{0.15-M}$, $^{13}C_{0.28}$, and $^{13}C_{0.82}$ enriched inner tubes at $\lambda=676$ nm laser excitation and 90 K measured with high resolution. Vertical dashed lines are intended to guide the eye. The decomposition of the 15 separate RBM lines in the $^{\text{nat}}C$ spectrum is also plotted below the measured spectrum with dashed lines.

In Fig. 2 we show the Raman spectra of DWCNTs based on $^{\text{nat}}C_{60}$, $^{13}C_{0.15-M}$, $^{13}C_{0.28}$, and $^{13}C_{0.82}$ peapods ($^{\text{nat}}C$-, $^{13}C_{0.15-M}$-, $^{13}C_{0.28}$-, and $^{13}C_{0.82}$-DWCNT) for the RBM. The spectra shown were taken at $\lambda=676$ nm laser excitation. This laser excitation provides the best resolution, but the spectra taken with other lasers in the visible range were all consistent with the presented spectra. Note that while the resonance condition selects a small number of inner tubes which contribute to the Raman signal at a given laser excitation, there are a large number of components. The observed Raman band consists of 15 separate lines altogether. This is plotted in the case of the $^{\text{nat}}C$-DWCNT sample in Fig. 2. The explanation of the large number of components is related to the interwall interaction; we discuss this briefly in the next section. The overall downshift and the broadening of the RBMs for the uniform filling produced samples were

observed previously.[7] The downshift is related to the heavier mass of the ^{13}C nuclei compared to the more abundant ^{12}C. As reported in Ref. 7, the spectra contain a Gaussian component even after deconvolution of the Gaussian response of the spectrometer, showing that there is an additional Gaussian broadening effect, related to the inhomogeneous distribution of the different isotopes. Both effects were also quantitatively explained by first-principles methods. It was also shown in Ref. 7 that a simple continuum model, i.e., considering the inner tube walls as simply heavier due to the presence of the ^{13}C isotopes, gives a good description of the center of the tube resonances and $(\nu_0-\nu)/\nu_0=1-\sqrt{\frac{12+c_0}{12+c}}$. Here, ν_0 and ν are the Raman shifts of the same inner tube mode in the natural carbon and enriched materials, respectively, and $c_0=0.011$ is the natural abundance of ^{13}C in carbon. The Raman shifts can be determined by fitting Voigtian line shapes to the lines. We obtained $c=27.7(7)$, $c=82.4(8)$, and $c=14.7(6)$ for the $^{13}C_{0.28}$-, $^{13}C_{0.82}$-, and $^{13}C_{0.15-M}$-DWCNT samples, respectively.

In the previous work of Ref. 7, the broadening was found to follow a parabolalike function with a maximum at $c=0.5$. This suggests that at $c=0.15$, a smaller broadening is expected than at $c=0.28$. However, as shown in Fig. 2, a significantly larger broadening was observed for this sample. As we will show below, these findings clearly suggest the absence of carbon diffusion along the tube axis during inner tube growth and are a strong support of inner tube growth through Stone-Wales transformations from interconnected fullerenes.

IV. RESULTS

Using the method detailed above, we have calculated the inhomogeneous broadening of the RBM frequency of the (10,0), (7,4), and (5,5) SWCNTs.

In the case of the uniform filling method, the ^{13}C isotopes are uniformly distributed in the supercell along the tube axis: the ^{13}C nuclei are randomly placed within the entire supercell, with no predefined nonenriched regions (as opposed to the mixed filling calculations below). To ensure that the considered configurations give a good statistics, we divided the supercells into 60-atom sections [62 in the case of the (7,4) tube], in which the enrichment level was restricted to correspond to the average enrichment level. This ensured that the spatial distribution of isotopes along the tube axis stays largely uniform even in the case of long supercells. Each section was treated separately with a random distribution of its own; only the enrichment level was the same for all sections.

We have calculated the inhomogeneous Gaussian broadening for 10%, 30%, 50%, 70%, and 90% ^{13}C content for all three tubes. The results are depicted in the lower part of Fig. 3. As expected, in all three cases the broadening increases with increasing level of enrichment until ^{13}C content reaches 50%, where the broadening has a maximum. These results qualitatively agree with our earlier work in Ref. 7, where we calculated the broadening for a (5,5) tube using the unit cell only. However, the current data give a smaller broadening. The use of supercells in the current calculation improves the result since the calculation of the Hessian is much more accurate as long-range force constants are taken into account. In addition, the use of a larger supercell allows for a higher degree of freedom when generating the random isotope distributions. In this work, we used large supercells for constructing the dynamical matrix. For the (7,4) and (5,5) calculations, we used supercell lengths of 27.2 Å (two unit cells) and 29.4 Å (12 unit cells), respectively. In the case of (10,0), we have performed the calculation at different supercell sizes—25.4 Å (six unit cells), 38.1 Å (nine unit cells), and 50.8 Å (12 unit cells)—to see how the broadening changes with the supercell size. We have found that the data points deviate within an error bar of 0.05 cm^{-1}; this is depicted in the figure.

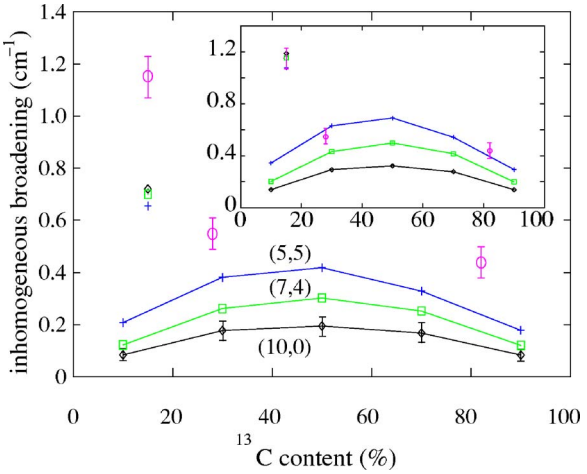

FIG. 3. (Color online) Calculated inhomogeneous broadening of the RBM mode of the (10,0), (7,4), and (5,5) SWCNTs (diamonds, squares, and crosses, respectively), compared with measurements (circles). All values are full width at half maximum. The results in the lower part of the figure show the case of uniform filling derived DWCNTs, while the few data points in the upper left corner are the case of mixed filling derived tubes. The error bars on the data points of (10,0) depict the variance of the broadening as a function of supercell size. The inset shows exactly the same data except that the calculated results are upscaled by a factor of 1.65 (see text).

There is a difference in the magnitude of the broadening of the three different tubes, and the difference is clearly larger than the error bar of the data points. This suggests that the magnitude of the inhomogeneous broadening is slightly chirality dependent in the case of DWCNTs based on the uniform filling method. Note that the experimental broadening shown in Fig. 3 is about 1.5–2 times larger than what is obtained theoretically.

As mentioned above, a new and interesting experimental finding is that the inhomogeneous Gaussian broadening was found to be larger for the $^{13}C_{0.15-M}$-DWCNT sample than for the $^{13}C_{0.28}$-DWCNT sample, and the $^{13}C_{0.82}$-DWCNT sample. Given that the calculations clearly predict that the broadening monotonically increases from 0% enrichment to 50% enrichment, the broadening should be smaller for a 15% average enrichment level than both for a 28% average enrichment level and a 82% average enrichment level.

These experiments suggest that the local enrichment level changes along the tube axis in the $^{13}C_{0.15-M}$-DWCNT

sample, as opposed to the $^{13}C_{0.28}$-DWCNT sample. More specifically, the experiments suggest that the carbon atoms do not exhibit large diffusion along the tube axis during the creation of the inner tube; thus, the local enrichment level of the nanotube reflects the local enrichment of the original filling material. To test this assumption, we have performed calculations for an average enrichment level of 15%, but assuming that the nanotube is composed of enriched (30%) and nonenriched (0%) sections, which follow each other randomly. We assumed that the ratio of enriched and nonenriched sections is 1:1 and that the sections have the size of 60 atoms [62 in the case of the (7,4) nanotube due to the unit cell size], which closely models the experimentally realized samples.

The length of the supercell was eight sections for all three tubes—50.8 Å (12 unit cells and 480 atoms), 54.4 Å (four unit cells and 496 atoms), and 58.8 Å (24 unit cells and 480 atoms) for (10,0), (7,4), and (5,5), respectively—ensuring a large enough variety in the order of different kinds of sections within the supercell. The spatial distribution of isotopes within an enriched section was random just like in the case of the uniform calculations above, and each enriched section within the supercell was given a different random distribution of its own. Note that the sections defined here are the same as those defined in the uniform calculations above, and that this construction of the supercells ensures that the sets of random configurations used in the two kinds of calculations at the same average enrichment level are disjunct.

The results of the calculation are depicted in the upper left corner of Fig. 3, showing that the calculations are in very good qualitative agreement with the experiments: a significantly larger broadening is found than in the case of the uniform filling derived DWCNTs discussed above. The calculated data points all fall within the error bar of the calculations; thus, this effect shows no chirality dependence, as opposed to the case of uniform filling derived tubes. In other words, the calculation predicts that any chirality dependence of the inhomogeneous broadening is smeared out if the mixed filling method is used instead of the uniform filling method.

The magnitude of the broadening is once again underestimated by a factor of 1.5–2. If the calculated results are upscaled by a factor of 1.65, then all calculated values for the mixed filling derived DWCNTs fall within the error bar around the experimentally obtained value. At the same time, the theoretical results on the uniform filling derived (5,5) inner tube also match the experimental results after the same upscaling, which shows that the relative increase of the inhomogeneous broadening for this tube is in excellent agreement with the experiments. This is illustrated in the inset of Fig. 3.

One thing should be noted about comparison with the experiments. According to the identification method based on the so-called Raman map of laser excitations, the 15 lines observed in the experiment originate from (n,m) nanotubes for which $(2n+m)=19$ (see Ref. 36). The diameter range of the inner tubes restricts the number of possible chiralities to four nanotubes: (7,6), (7,5), (8,3), and (9,1). The 15 observed lines are contributions of these four inner tubes. (The reason there are more than just four lines is that the interaction with the outer wall causes a shift of the inner tube RBM frequency, and this shift depends on the chirality of the outer tube, thus resulting in the appearance of more than one RBM line per inner tube.[36]) For the most direct comparison with the experiments, one would need to perform the calculations on these four nanotubes. However, their unit cell size ($\sim$300–500 atoms) is too large to handle with the VASP code, and it is not possible to calculate the Hessian matrix with sufficient accuracy. However, the three tubes we examined give a good and representative selection of the possible chiralities and diameters in the sample. Given that—as we discuss below—we do not find a strong chirality dependence experimentally, these three tubes serve the purpose of comparing theory and experiment very well.

V. DISCUSSION

A. Qualitative arguments

A simple qualitative argument can be given for the increased broadening in the case of the mixed filling derived tubes.

What must first be realized is that the cases of mixed and uniform filling are largely different. The physical restriction of negligible diffusion renders the set of possible configurations in the two cases disjunct. While in principle a largely uniform isotope distribution may occur even in the case of mixed filling, the low diffusion makes the probability of this negligible. Likewise, uniform filling is unlikely to produce a largely nonuniform isotope distribution.

This disjunctness was strongly included in our calculations. As written above, by the use of appropriately defined sections within the supercells, we restricted the calculations such that no uniform distribution may occur in the case of mixed filling, and we likewise excluded the possibility of a mixed configuration from the calculations on the uniform filling derived tubes.

Due to the applied restrictions we used to describe the physical difference between the case of uniform and mixed filling, one immediately expects to find a qualitatively different behavior in the two cases. Furthermore, one can argue that in the case of mixed filling, a larger broadening is expected even based on qualitative assumptions. The presence of enriched and nonenriched sections along the tube axis creates a larger inhomogeneity of the spatial distribution of carbon isotopes. This suggests that the vibrational modes are very likely to suffer a larger distortion in the case of mixed filling than in the case of uniform filling. A larger distortion of the modes can also have a larger effect on the vibrational frequencies, and therefore can lead to a larger average deviation of the frequencies from their mean values.

This qualitative argument already suggests that the mixed filling results in a larger inhomogeneous broadening. Our calculations detailed above are in agreement with this qualitative argument, as the vibrational modes in the case of mixed filling are indeed more distorted than in the case of uniform filling. The distortion can be quantitatively described by the scalar product square of the modes with the mode corresponding to true radial movement (which was used to provide weight factors for each mode, as detailed

above). The maximum of this value was between 0.8 and 0.85 for the least distorted modes in the case of mixed filling, while in the case of uniform filling, it was between 0.9 and 0.95, showing that indeed the modes are more distorted in the case of mixed filling, supporting the qualitative argument described above.

B. Underestimation of the broadening

As detailed above, our calculations are in good qualitative agreement with the experiments, but the calculations underestimate the experimental broadening by a factor of 1.5–2. During the calculations, certain restrictions were necessarily made. The most significant restricting factor is the presence of periodic boundary conditions (PBC). In a real experiment, the different isotopes in a nanotube are distributed totally randomly. However, in the calculation, it is made periodic by PBC, and true randomness is only realized within the supercell. This restriction can lead to a reduction of the magnitude of the inhomogeneous broadening of the Raman lines, thereby resulting in an underestimation of the experimental broadening. Basically, the periodic boundary conditions imply that there is no fluctuation of the local enrichment level and the random distribution of isotopes in sections along the tube axis if the section size exceeds the supercell sizes used, while normally there should be some fluctuation which should increase the broadening.

This fluctuation originates from the binomial distribution of ^{13}C enrichment level in the fullerenes. Since the inner tube inherits the local enrichment level of the fullerenes from which it was produced, it should reflect the binomial distribution of ^{13}C enrichment level in the fullerenes, leading to the aforementioned fluctuation. Therefore, this extra broadening effect is analogous to the broadening effect of the binomial distribution of different isotope distributions of ^{13}C-enriched C_{60}. In other words, enforcing periodic boundary conditions in a nanotube is analogous to restricting the enrichment level of C_{60} molecules to the mean value, which results in a decrease of the total Raman linewidths. For example, the broadening of the Raman lines of a 10% ^{13}C-enriched C_{60} sample is not solely determined by the inhomogeneous distribution of isotopes in a $^{13}C_6{}^{12}C_{54}$ molecule, but it is also increased by the appearance of $^{13}C_5{}^{12}C_{55}$, $^{13}C_7{}^{12}C_{53}$, etc., molecules in the sample, as determined by the binomial distribution. We have made a test calculation to determine this effect in the case of a 10% ^{13}C-enriched C_{60} sample. The calculation was performed similar to the nanotubes. The Hessian was obtained by the GAUSSIAN program package. We have found that the inclusion of the broadening effect of the binomial distribution increases the total broadening of the Raman pinch and RBM modes by 30%, showing that neglecting this effect results in a significant reduction of the total broadening. Due to the analogy between this effect and the role of periodic boundary conditions in the case of the nanotubes, we expect that enforcing periodic boundary conditions leads to an underestimation of the broadening. However, the magnitude and the chirality dependences (if any) of the necessary correction are difficult to estimate.

There are other effects which are neglected in the calculation and which may contribute to the broadening, such as the possibility of the increase of the natural Raman linewidth with isotope enrichment, which would further increase the linewidth. The significance of this particular effect is very easy to illustrate in the case of C_{60}. In a work by Guha *et al.*,[37] the Raman line of the pinch mode of C_{60} made of natural carbon was resolved to three components, corresponding to the contributions of $^{12}C_{60}$, $^{13}C^{12}C_{59}$, and $^{13}C_2{}^{12}C_{58}$. In their measurements, it is clearly shown that the natural linewidth of $^{13}C^{12}C_{59}$ is 10% larger than that of $^{12}C_{60}$. A similar effect may occur in the case of nanotubes as well, but its magnitude is difficult to estimate.

One more possible source of extra broadening which we cannot take into account is the broadening of the anharmonic correction. Anharmonic effects are expected to have very small effects on the RBM mode, as the harmonic approximation has proven to fit well to the energy surface around the optimal geometry (see e.g. Ref. 29). However, though the anharmonic correction to the frequency may be very small, it will suffer a broadening due to the random distribution of isotopes much like the frequencies obtained within the harmonic approximation. While we would not expect the relative broadening of the anharmonic correction to be larger than that of the harmonic frequency and so we would expect the associated broadening to be negligible next to the broadening of the harmonic frequency, we cannot completely outrule the influence of anharmonicity on the broadening of the RBM band; hence, this effect may also be a possible source of our underestimation of the measured isotopic broadening.

C. Chirality dependence

The theoretically found chirality dependence of the inhomogeneous broadening in the case of uniform filling derived DWCNTs shows a very clear trend: the broadening is largest for the examined armchair tube, smallest for the examined zigzag tube, and the examined chiral tube falls in between, suggesting that the broadening decreases as one changes the chiral angle and goes from armchair to zigzag nanotubes. However, the predicted chirality dependence is rather small, with the spread of the data points being on the order of $0.3–0.4\ cm^{-1}$, which is the limit of the experimental precision to determine the inhomogeneous broadening, as shown by the error bar in Fig. 3. Experimentally, we did not detect any systematic inhomogeneous broadening which could be related to chirality effects, although the chiral indexing is available for inner tubes.[36] It is also possible that this chirality dependence is an artifact of the calculation and is in connection with the neglections detailed above. It is interesting to note, however, that since there is no chirality dependence in the case of the calculations on the mixed filling derived DWCNTs, if the chirality dependence is indeed an artifact then the factors which produce this artifact are somehow averaged out in the case of the mixed filling derived tubes.

D. Absence of carbon diffusion

Finally, we discuss the relevance of our study to the inner tube growth mechanism.

As detailed above, the good agreement between the experimental and calculated inhomogeneous broadening for the

inner tubes made from mixed enriched and natural fullerenes is a clear indication that there is very little diffusion of carbon atoms along the tube axis during the creation of the inner tube in the peapod-to-DWCNT transformation process.

This result implies that the inner tubes grow with a mechanism that does not require a full disintegration of the fullerenes which would inevitably involve mixing and diffusion of carbons along the tube axis. Rather, carbons are pinned to the location of the original fullerenes. An inner tube growth mechanism, which satisfies this experimental observation, was suggested in Refs. 21–23. It was found using molecular-dynamics calculations that in the first step of inner tube growth, covalently bound fullerenes are formed as precursors. In addition, Bandow *et al.* found using transmission electron microscopy that inner tube precursors are indeed short fullerene dimer or oligomer sections.[23] These structures can then proceed toward short inner tube sections with low-energy Stone-Wales transformations. This mechanism certainly provides that carbons remain on the original location of the starting fullerenes. Thus, the current data are a strong support for this mechanism.

Alternative models considered the inner tube growth from completely disintegrated fullerenes into, e.g., C_2 units.[25] However, in this model strong carbon diffusion along the tube axis would be expected, which means that the carbon isotopes could spread along the tube axis, thereby resulting in a more or less uniform isotope distribution even if it was not uniform in the starting peapod material. Our results, however, show that there is practically no diffusion, which suggests that the growth of the inner tube does not occur by a complete disintegration of the fullerenes, but rather by a Stone-Wales-type fusion mechanism.

The current result also shows that inner tubes grown from the mixture of enriched and nonenriched fullerenes contain randomly alternating ^{13}C rich and poor sections along the tube axis. This is an interesting architecture and as such has been suggested as a building element for quantum computing with nuclear spins.[38] Exploitation of this would certainly require more controlled arrangement of the ^{13}C rich and poor regions, which is currently unavailable.

VI. CONCLUSIONS

We have performed first-principles calculations on the inhomogeneous broadening of the Raman RBM lines of isotope-engineered double-walled carbon nanotubes and compared the calculations to our experimental results. We have shown that the broadening grows monotonically with increasing enrichment and peaks at 50% ^{13}C content. We have found experimentally that if the filling of the peapod is performed with a mixture of enriched and nonenriched fullerenes, the Raman spectra of the resulting inner tubes show a much larger broadening than in the case of the uniform filling method. Our calculations have shown that this finding is consistent with the assumption that the local enrichment level of the double-walled tube reflects the local enrichment level of the corresponding peapod material. Good agreement between our calculations and experiments clearly indicates that there is very little diffusion of carbon atoms along the tube axis, supporting the theory that the inner tubes are formed by Stone-Wales transformations from interconnected fullerenes.

ACKNOWLEDGMENTS

This work was supported by OTKA Grants Nos. K60576, T043685, TS049881, F61733, NK60984, and FWF I83-N20 (ESF IMPRESS) in Hungary, by the Austrian Science Funds (FWF) No. 17345, and by the EU projects HPRN-CT-2002-00192 and MERG-CT-2005-022103. F.S. acknowledges the Zoltán Magyary postdoctoral program.

[1] J. Bardeen, L. N. Cooper, and J. R. Schrieffer, Phys. Rev. **108**, 1175 (1957).
[2] M. C. Martin, J. Fabian, J. Godard, P. Bernier, J. M. Lambert, and L. Mihály, Phys. Rev. B **51**, 2844 (1995).
[3] A. Rosenberg and C. Kendziora, Phys. Rev. B **51**, 9321 (1995).
[4] P. J. Horoyski, M. L. W. Thewalt, and T. R. Anthony, Phys. Rev. B **54**, 920 (1996).
[5] W. S. Capinski, H. J. Maris, E. Bauser, I. Silier, M. Asen-Palmer, T. Ruf, M. Cardona, and E. Gmelin, Appl. Phys. Lett. **71**, 2109 (1997).
[6] Y. Li, U. Rayaioli, and S. V. Rotkin, Phys. Rev. B **73**, 035415 (2006).
[7] F. Simon, C. Kramberger, R. Pfeiffer, H. Kuzmany, V. Zólyomi, J. Kürti, P. M. Singer, and H. Alloul, Phys. Rev. Lett. **95**, 017401 (2005).
[8] P. M. Singer, P. Wzietek, H. Alloul, F. Simon, and H. Kuzmany, Phys. Rev. Lett. **95**, 236403 (2005).
[9] S. Iijima and T. Ichimashi, Nature (London) **363**, 603 (1993).
[10] D. S. Bethune, Nature (London) **363**, 605 (1993).
[11] C. D. Spataru, S. Ismail-Beigi, L. X. Benedict, and S. G. Louie, Phys. Rev. Lett. **92**, 077402 (2004).
[12] F. Wang, G. Dukovic, L. E. Brus, and T. F. Heinz, Science **308**, 838 (2005).
[13] Z. K. Tang, L. Y. Zhang, N. Wang, X. X. Zhang, G. H. Wen, G. D. Li, J. N. Wang, C. T. Chan, and P. Sheng, Science **292**, 2462 (2001).
[14] H. Ishii, H. Kataura, H. Shiozawa, H. Yoshioka, H. Otsubo, Y. Takayama, T. Miyahara, S. Suzuki, Y. Achiba, M. Nakatake *et al.*, Nature (London) **426**, 540 (2003).
[15] H. Rauf, T. Pichler, M. Knupfer, J. Fink, and H. Kataura, Phys. Rev. Lett. **93**, 096805 (2004).
[16] K. P. Bohnen, R. Heid, H. J. Liu, and C. T. Chan, Phys. Rev. Lett. **93**, 245501 (2004).
[17] D. Connétable, G.-M. Rignanese, J.-C. Charlier, and X. Blase, Phys. Rev. Lett. **94**, 015503 (2005).
[18] X.-P. Tang, A. Kleinhammes, H. Shimoda, L. Fleming, K. Y. Bennoune, S. Sinha, C. Bower, O. Zhou, and Y. Wu, Science **288**, 492 (2000).
[19] C. Goze-Bac, S. Latil, P. Lauginie, V. Jourdain, J. Conard, L. Duclaux, A. Rubio, and P. Bernier, Carbon **40**, 1825 (2002).

[20] R. Pfeiffer, H. Kuzmany, C. Kramberger, C. Schaman, T. Pichler, H. Kataura, Y. Achiba, J. Kürti, and V. Zólyomi, Phys. Rev. Lett. **90**, 225501 (2003).
[21] Y. Zhao, B. I. Yakobson, and R. E. Smalley, Phys. Rev. Lett. **88**, 185501 (2002).
[22] S. W. Han, M. Yoon, S. Berber, N. Park, E. Osawa, J. Ihm, and D. Tománek, Phys. Rev. B **70**, 113402 (2004).
[23] S. Bandow, T. Hiraoka, T. Yumura, K. Hirahara, H. Shinohara, and S. Iijima, Chem. Phys. Lett. **384**, 320 (2004).
[24] A. J. Stone and D. J. Wales, Chem. Phys. Lett. **128**, 501 (1986).
[25] F. Simon, A. Kukovecz, C. Kramberger, R. Pfeiffer, F. Hasi, H. Kuzmany, and H. Kataura, Phys. Rev. B **71**, 165439 (2005).
[26] G. Kresse and J. Hafner, Phys. Rev. B **48**, 13115 (1993).
[27] G. Kresse and J. Furthmüller, Comput. Mater. Sci. **6**, 15 (1996).
[28] G. Kresse and J. Furthmüller, Phys. Rev. B **54**, 11169 (1996).
[29] J. Kürti, V. Zólyomi, M. Kertesz, and G. Sun, New J. Phys. **5**, 125 (2003).
[30] O. Dubay and G. Kresse, Carbon **42**, 977 (2004).
[31] M. J. Frisch, G. W. Trucks, H. B. Schlegel, G. E. Scuseria, M. A. Robb, J. R. Cheeseman, J. A. Montgomery, Jr., T. Vreven, K. N. Kudin *et al.*, GAUSSIAN 03, Gaussian, Inc., Wallingford, CT, 2003.
[32] http://www.nanocarblab.com
[33] H. Kuzmany, W. Plank, M. Hulman, C. Kramberger, A. Grüneis, T. Pichler, H. Peterlik, H. Kataura, and Y. Achiba, Eur. Phys. J. B **22**, 307 (2001).
[34] H. Kataura, Y. Maniwa, T. Kodama, K. Kikuchi, K. Hirahara, K. Suenaga, S. Iijima, S. Suzuki, Y. Achiba, and W. Krätschmer, Synth. Met. **121**, 1195 (2001).
[35] S. Bandow, M. Takizawa, K. Hirahara, M. Yudasaka, and S. Iijima, Chem. Phys. Lett. **337**, 48 (2001).
[36] R. Pfeiffer, F. Simon, H. Kuzmany, and V. N. Popov, Phys. Rev. B **72**, 161404(R) (2005).
[37] S. Guha, J. Menendez, J. B. Page, G. B. Adams, G. S. Spencer, J. P. Lehman, P. Giannozzi, and S. Baroni, Phys. Rev. Lett. **72**, 3359 (1994).
[38] I. Shlimak, HAIT J. Sci. Eng. **1**, 196 (2004).